Desalination and Water Treatment
www.deswater.com
doi: 10.5004/dwt.2021.26367

209 (2021) 219–229
January

Optimization and modeling of the photocatalytic activities of a novel visible driven CNT/TiO_2/BiOBr/Bi_2S_3 nanocomposite

M. Asadpoor[a], M. Arjmand[a,*], M. Farhadian[b], M.R. Omidkhah[c], A.A. Zinatizadeh[d,e]

[a]*Department of Polymer and Chemical Engineering, Islamic Azad University, South Tehran Branch, Tehran, Iran, emails: mehdi.arjmand2020@yahoo.com (M. Arjmand), malihe_asadpoor@yahoo.com (M. Asadpoor)*
[b]*Department of Chemical Engineering, Faculty of Engineering, University of Isfahan, Isfahan, Iran, emails: mehrdadfarhadian@yahoo.com/m.farhadian@eng.ui.ac.ir (M. Farhadian)*
[c]*Department of Chemical Engineering, Faculty of Chemical Engineering, Tarbiat Modares University, Tehran, Iran, email: Omidkhah@modares.ac.ir (M.R. Omidkhah)*
[d]*Environmental Research Center (ERC), Department of Applied Chemistry, Razi University, P.O. Box: 67149, Kermanshah, Iran, email: zinatizadeh@gmail.com (A.A. Zinatizadeh)*
[e]*Department of Environmental Sciences, University of South Africa, Pretoria, South Africa*

Received 9 October 2019; Accepted 14 July 2020

ABSTRACT

In this work, the photocatalytic degradation of Acid black 1721 (AB1721) in the presence of a novel photocatalyst (TiO_2 – titanium dioxide) TiO_2/CNT/BiOBr/Bi_2S_3 under visible light irradiation was investigated. The effect of different loadings of carbon nanotubes (CNT) (1%, 2%, 4%, 6% and 8%), BiOBr (10, 20, 30 and 40 wt.%) and Bi_2S_3 (5, 10, 15 and 20 wt.%) on the photocatalytic activities of the prepared nanocomposites was investigated. The structural properties of the nanocomposites have been characterized by X-ray diffraction, Brunauer–Emmett–Teller, diffuse reflectance spectra (DRS), Field-emission scanning electron microscopy, photoluminescence spectroscopy (PL) and Fourier-transform infrared spectroscopy. The results show that the photodegradation efficiency of TiO_2/4-CNT/20-BiOBr/10-Bi_2S_3 photocatalyst was better than the samples. Results of DRS show a visible shift when TiO_2/CNT was modified with BiOBr and Bi_2S_3. Also, PL spectra for all the prepared samples indicated that TiO_2/4-CNT/20-BiOBr/10-Bi_2S_3 had the lowest recombining of electron and holes. The effect of independent variables including initial dye concentration (30, 60 and 90 mg/L), pH (3, 6 and 9), irradiation time (20, 30 and 40 min) and catalyst loading (0.5, 0.75 and 1 g/L) on dye removal was determined by response surface methodology. The optimum condition was AB1721 concentration of 30 mg/L, initial pH of 3, the reaction time of 40 min, and catalyst loading of 1 g/L.

Keywords: CNT/TiO_2/BiOBr/Bi_2S_3 nanocomposite; Photocatalyst; Acid black 1721; Visible light

1. Introduction

The dyes especially azo dyes are important pollutants in wastewaters, which are mainly discharged from industries like textile, printing, food, leather, plastics, cosmetics and etc [1]. Removal of color from wastes is often more important than the other organic substances because even the presence of small amounts of dyes (below 1 ppm) is clearly visible and influences the water environment considerably [1,2]. The biological treatment processes are costly, inefficient or produce secondary toxic products to remove dye from water and wastewater. The physical and chemical treatment processes such as adsorption, membrane filtration (ultrafiltration and reverse osmosis), coagulation/

* Corresponding author.

flocculation and sedimentation are non-destructive which they transfer the organic pollutions to another phase and produce solid-wastes [2,3]. The tremendous developments and researches have been recently done to find an inexpensive and safe method to remove dye pollutants from water and wastewater. Photocatalytic processes are a class of advanced oxidation processes (AOP). Among the viable AOPs, the use of a heterogeneous photocatalytic system using semiconductor photocatalysts has become one of the most favorable methods [1]. Photocatalytic degradation of recalcitrant compounds especially dyes are widely accomplished in water and wastewater treatment due to the complete mineralization of organic pollutions to H_2O and CO_2 under mild temperature and pressure [3].

Titanium dioxide (TiO_2) is an important semiconductor material, which has attracted attention due to its advantages including broad source, little contamination, high chemical stability low cost and non-toxicity [3,4]. One of its main applications is to act as photocatalyst for the treatment of water polluted with organic and inorganic pollutants. The main drawback of the use of TiO_2 as photocatalyst is its wide band-gap as well as relatively fast recombination rate of electron-hole pairs [5]. The photocatalytic efficiency of TiO_2 powder heavily depends on its microstructure and physical properties, which are in turn determined by the preparation conditions [6]. To overcome the defect, different modifications have been done. To achieve this aim, many attempts have been made such as the design of nanoporous structures, construction of heterostructures and chemical doping [1,4]. Carbon nanotubes (CNTs) have recently been determined because of their to be more attractive catalyst supports than activated carbons, a combination of electronic, adsorption, mechanical and thermal properties [6–8]. CNTs have been reported to synergistically enhance the photocatalytic efficiency of TiO_2 and therefore may accept photogenerated electrons in TiO_2, thus reducing the recombination [9,10].

In order to improve the sunlight utilization efficiency and separation of photoinduced electron and hole pairs, bismuth oxyhalide compounds BiOX (X = Cl, Br, and I) have been widely studied for their high photocatalytic activity under visible light in recent years [10–14]. Bismuth oxybromide (BiOBr) is a new type of promising photocatalyst and has attracted much attention in recent years because of its, eco-friendly qualities, suitable bandgap and good chemical stability [15–18]. However, the unitary sensitization role is hardly competent for maximizing the charge-carrier separation, so Bi_2S_3 as an attractive semiconductor due to its high photo-electron conversion efficiency and narrow bandgap (E_g = 1.3 eV) was coupled with CNT/TiO_2/BiOBr to enhance its quantum efficiency [11,19]. The combination of Bi_2S_3 with TiO_2 produces the photocatalyst TiO_2/Bi_2S_3 that could absorb the full visible light area contributing 45% of the solar spectrum [19].

In this study, the CNT/TiO_2, CNT/TiO_2/BiOBr and CNT/TiO_2/BiOBr/Bi_2S_3 nanophotocatalysts were synthesized and their properties were identified using Field-emission scanning electron microscopy (FE-SEM)/energy-dispersive X-ray (EDX), X-ray diffraction (XRD), Fourier-transform infrared spectroscopy (FTIR), diffuse reflectance spectra (DRS) and photoluminescence spectroscopy (PL) analyses. The prepared nanophotocatalysts were applied for the photocatalytic removal of Acid black 1721 (AB1721) dye from water in a suspended photoreactor. The photocatalytic degradation of AB1721 was modeled and optimized using central composite design (CCD) based on response surface methodology (RSM). The effect of dye concentration, photocatalyst concentration, pH and irradiation time on the AB1721 photodegradation process was also studied by CCD.

2. Experimental setup

2.1. General

The solvents and reagents used in this study were achieved from Aldrich or Merck (Germany) and were used without purification. FE-SEM was examined using a Philips XL30 microscope (Company in The United States). FTIR was recorded in KBr on Shimadzu Varian 4300 spectrophotometer (company in Japan). The crystalline structure of the samples was investigated by a Rigaku D/Max C III, XRD using Ni-filtered Cu Kα radiation. The absorption spectra of photocatalysts were examined by UV-Vis spectrophotometer (Rayleigh UV-2601 model). The PL was identified by the photoluminescence spectrometer a photomultiplier tube (Perkin-Elmer LS-55, Company in The United States). Brunauer–Emmett–Teller (BET) surface areas were measured on a sorptometer Kelvin 1042 using nitrogen adsorption. Before the adsorption test, the samples were out-gassed at 150°C for 12 h, reaching a final pressure of 10^{-6} mbar.

2.2. Photodegradation of AB1721

Photodegradation experiments were done in a suspended glass photoreactor (Fig. 1). The used photoreactor has mainly three parts including reactor vessel (250 mL), fluorescent lamp (18 W, visible light source, λ > 420 nm) and plexiglass chamber that was filled with circulated water to control the temperature and reactor vessel was placed inside the chamber. The suspension of the solid catalyst was added to the dye solution. The prepared solution was then located in the dark condition for at least 30 min to ensure that the adsorption–desorption equilibrium, then the photoreactor was put under visible light irradiation. All experiments were done at room temperature. After different irradiation time, 3 mL of the treated solution was collected and immediately centrifuged to remove the suspended solids from the solution and photodegradation of AB1721 was identified by a UV-Vis spectrophotometer at 572 nm. The initial pH of pollution was adjusted by a NaOH or HCl 0.1 M. The AB1721 photodegradation on efficiency (%) has been calculated according to the following equation:

$$R(\%) = \frac{C_0 - C_e}{C_0} \times 100 \quad (1)$$

where C_0 is the initial AB1721 concentration and C_e is the final AB1721 concentration after treating.

2.3. Experimental design

Optimum condition for the photodegradation of AB1721 was determined by RSM. RSM is a statistical method that

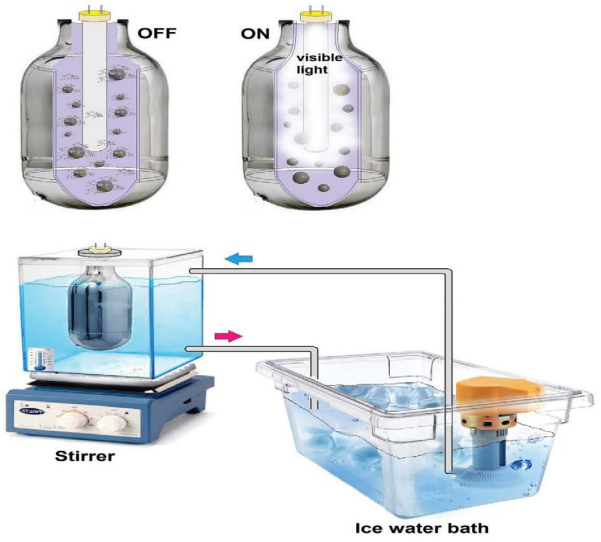

Fig. 1. Schematic image of the experimental photoreactor.

uses the quantitative data from experiments to examine the interaction of the several parameters affecting the process and study the responses of various *factors* by varying them simultaneously [20]. RSM has several classes of designs with different properties and features [21]. In this work, CCD was used to study the effect of four main variables on the photodegradation of AB1721. The range and the level of the variables including reaction time (20, 30 and 40 min), initial pH (3, 6, and 9), catalyst loading (0.5, 0.75 and 1 g/L) and initial dye concentration (30, 60 and 90 mg/L), that affect the photodegradation efficiency of AB1721 are presented in Table 1. A total of 30 tests were conducted in this work (Table 2).

2.4. Synthesis of TiO_2/a-CNT/b-BiOBr/c-Bi_2S_3

First, ethanol (10 mL) and acetic acid (0.8 mL) and various percentages of CNT (1, 2, 4, 6 and 8 wt.% (were mixed together under sonication for 15 min (solution 1). Then, tetrabutyl ortotitanate solution (1 mL) was added dropwise to the solution 1 and stirred for 1 h (solution 2). In the next step, different amounts of $Bi(NO_3)_3{\cdot}5H_2O$ (10, 20, 30 and 40 wt.% (and N-cetyl-N,N,N-trimethylammoniumbromide were added to absolute ethanol (10.0 mL) under sonication and stirred for 30 min. This solution is added dropwise to the solution 2 under sonication (solution 3). Next, different amounts of $Bi(NO_3)_3{\cdot}5H_2O$ (5, 10, 15 and 20 wt.% (and thiourea were added to absolute ethanol (10.0 mL) under sonication for 30 min and stirred for 30 min. This solution was added dropwise to solution 3 and stirred continuously for 30 min. The final solution was diluted with ethanol and transferred to the autoclave at 120°C for 24 h. The prepared catalyst was washed with a mixture of water and ethanol (3 times) and dried at 100°C for 12 h. Then, it was calcined at 400°C for 5 h. The obtained photocatalyst was denoted as TiO_2/*a*-CNT/*b*-BiOBr/*c*-Bi_2S_3, in which *a*, *b* and *c* represented the loading amount (wt.%) of CNT, BiOBr and Bi_2S_3 in the composite photocatalyst, respectively.

Table 1
Independent variables and their levels for the design of the tests

Parameter name	Symbols	Low	High
Initial concentration, mg/L	*A*	30	90
Catalyst dosage, g/L	*B*	0.5	1
pH	*C*	3	9
Reaction time, min	*D*	30	90

3. Result and discussion

3.1. Characterization of prepared nanocomposites

The FTIR spectra TiO_2/4-CNT, TiO_2/4-CNT/20-BiOBr and TiO_2/4-CNT/20-BiOBr/10-Bi_2S_3 nanocomposites are shown in Figs. 2a–c. The broad absorption band around 3,400 cm^{-1} is related to the stretching and bending mode of O–H groups and surface adsorbed water on the catalyst surface [22]. The peaks in the region at 460 and 1,640 cm^{-1} are corresponding to (Ti–O or Ti–O–Ti) bonding and carbonyl group, respectively [23].

The surface morphology of the prepared photocatalysts is visualized by FE-SEM, as shown in Fig. 3. FE-SEM images of the composite confirm that metal oxide nanoparticles grow directly with a uniform dispersion on individual CNT. The composite is composed of tube-like nanostructures forming an interlocked network from CNTs and TiO_2 nanoparticles. It was clearly seen that TiO_2 nanoparticles were coated on the surface of CNT and the CNT were dispersed homogeneously with an apparent agglomeration of the TiO_2 particles. Moreover, the chemical composition of TiO_2/4-CNT/20-BiOBr/10-Bi_2S_3 was also identified by EDX (Fig. 4). Based on this analysis, the presence of Ti, O, P, Br and Bi in the structure of the TiO_2/4-CNT/20-BiOBr/10-Bi_2S_3 was verified. There is no trace of any other impurities found within the detection limit of the EDX.

Fig. 5 shows the XRD spectra of TiO_2/4-CNT, TiO_2/4-CNT/20-BiOBr, TiO_2/4-CNT/20-BiOBr/10-Bi_2S_3 nanocomosites to analyze their crystalline structures. The diffraction peaks located at (101), (103), (004), (112), (200), (105), (211), (204), (116), (220) and (215) at 2θ around 25.3°, 36.9°, 37.8°, 38.6°, 48.0°, 53.9°, 55.1°, 62.7°, 68.8°, 70.3° and 75.0° related to anatase structure. Also, a small peak around 2θ° = 26.4° can be assigned to CNTs [24]. Notably, as shown in Figs. 5b and c, no characteristics peaks of belonging to the separate BiOBr and BiO_2O_3 are shown in the TiO_2/4-CNT/10-BiOBr and TiO_2/4-CNT/20-BiOBr/10-Bi_2S_3 nanocomposites, which indicates BiOBr and BiO_2O_3 were highly dispersed throughout the TiO_2/CNT nanocomposite.

The BET surface areas of pure TiO_2 and TiO_2/4-CNT/20-BiOBr/10-Bi_2S_3 nanophotocatalysts are 26.22 and 100.98 m^2/g, respectively. These data reflect the significant enhancement in the surface area of the synthesized TiO_2/4-CNT/20-BiOBr/10-Bi_2S_3 composite compared to pure TiO_2. The optical properties of photocatalysts have a significant effect on their photocatalytic activity. UV-Vis spectra of TiO_2/4-CNT, TiO_2/4-CNT/20-BiOBr, TiO_2/4-CNT/20-BiOBr/10-Bi_2S_3 are shown in Fig. 6. The absorption edge of TiO_2/4-CNT/20-BiOBr, TiO_2/4-CNT/20-BiOBr/10-Bi_2S_3 gets shifted to a higher wavelength as compared to TiO_2/4-CNT and increase the absorption capacity for visible light irradiation.

Table 2
Experimental conditions for the photocatalytic process

Run	Dye concentration (mg/L)	Catalyst dosage (g/L)	pH	Time (min)	Degradation efficiency (%)
1	30	0.5	9	40	30
2	30	1	3	40	30
3	30	0.75	6	30	30
4	60	0.5	6	30	60
5	30	1	9	40	30
6	90	0.75	6	30	90
7	90	1	3	40	90
8	30	0.5	3	20	30
9	30	1	9	20	30
10	60	0.75	3	30	60
11	60	0.75	6	30	60
12	60	0.75	6	20	60
13	90	1	3	20	90
14	30	1	3	20	30
15	60	0.75	6	30	60
16	60	1	6	30	60
17	90	1	9	40	90
18	90	0.5	3	20	90
19	60	0.75	6	30	60
20	60	0.75	6	30	60
21	60	0.75	6	40	60
22	30	0.5	3	40	30
23	60	0.75	6	30	60
24	90	1	9	20	90
25	90	0.5	9	20	90
26	90	0.5	9	40	90
27	60	0.75	9	30	60
28	60	0.75	6	30	60
29	90	0.5	3	40	90
30	30	0.5	9	40	30

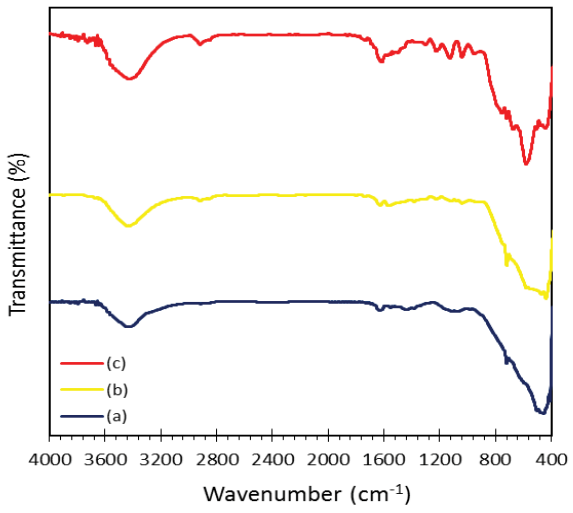

Fig. 2. FTIR spectra of (a) TiO_2/4-CNT, (b) TiO_2/4-CNT/20-BiOBr and (c) TiO_2/4-CNT/20-BiOBr/10-Bi_2S_3 nanocomposites.

The Tauc plots were used to estimate the bandgap of TiO_2, BiOBr, TiO_2/4-CNT, TiO_2/4-CNT/20-BiOBr, TiO_2/4-CNT/20-BiOBr/10-Bi_2S_3 which are obtained about 3.15, 2.6, 2.2, 1.78 and 1.5 eV, respectively. This can be attributed to the following reasons: the formation of Bi_2S_3-TiO_2 heterojunction leads to the notable increase in the light absorption [25] and BiOBr's lamellar structure which may allow the light to multi-reflect [26].

3.2. Optimization of CNT, BiOBr and Bi_2S_3 loadings in TiO_2 network

Figs. 7–9 show the photodegradation of AB1721 using prepared photocatalysts with different CNT dosage (1, 2, 4, 6 and 8 wt.%), BiOBr loading (10, 20, 30 and 40 wt.% (and Bi_2S_3 loading (5, 10, 15 and 20 wt.%. As shown in Figs. 8–10, the optimum loading (wt.%) of CNT, BiOBr and Bi_2S_3 were 4, 20 and 10 wt.%, respectively. It should be noted that the photocatalytic activity of TiO_2/4-CNT/20-BiOBr/10-Bi_2S_3

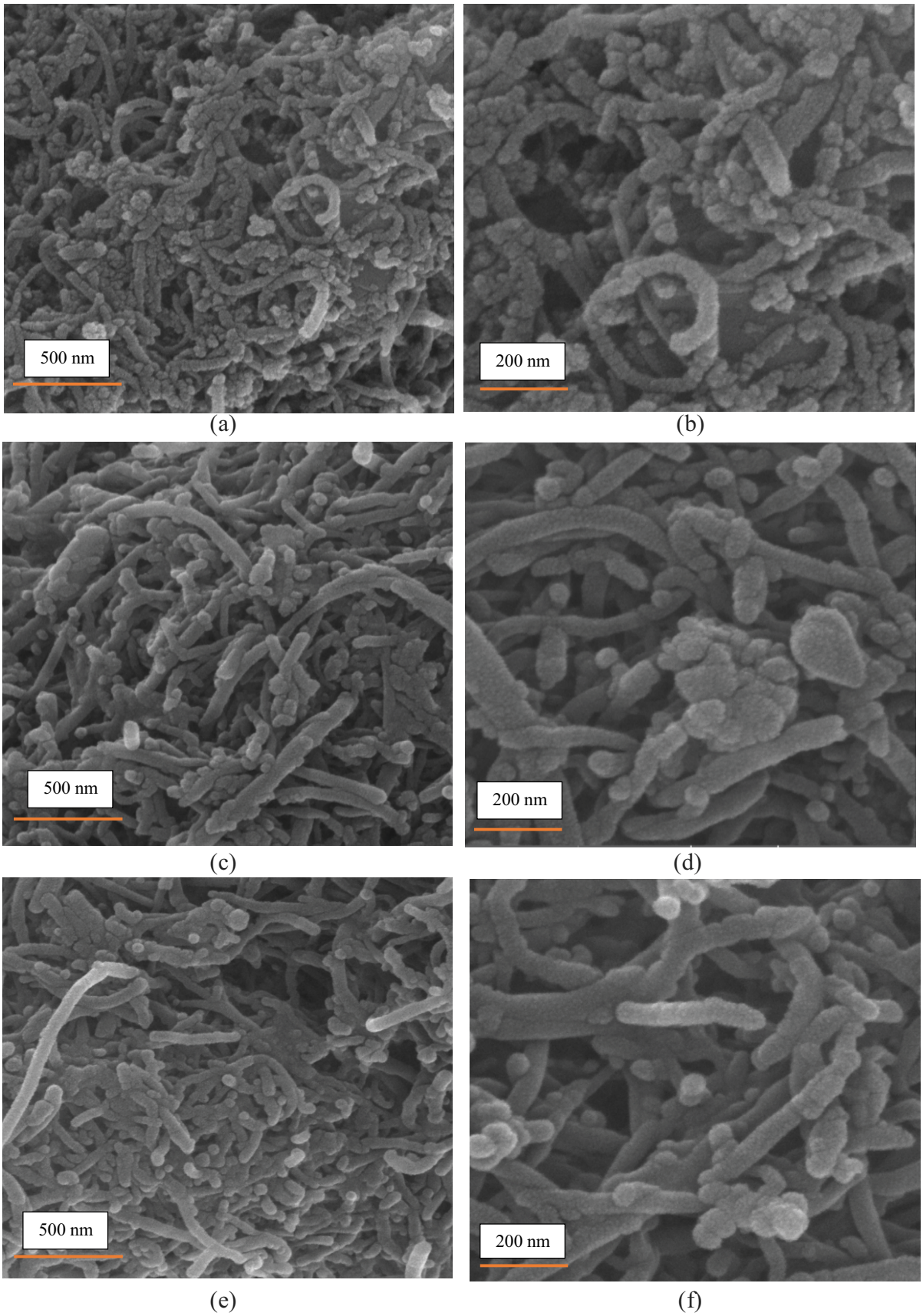

Fig. 3. FE-SEM images of (a–b) TiO_2/4-CNT, (c–d) TiO_2/4-CNT/20-BiOBr and (e–f) TiO_2/4-CNT/20-BiOBr/10-Bi_2S_3 nanocomposites.

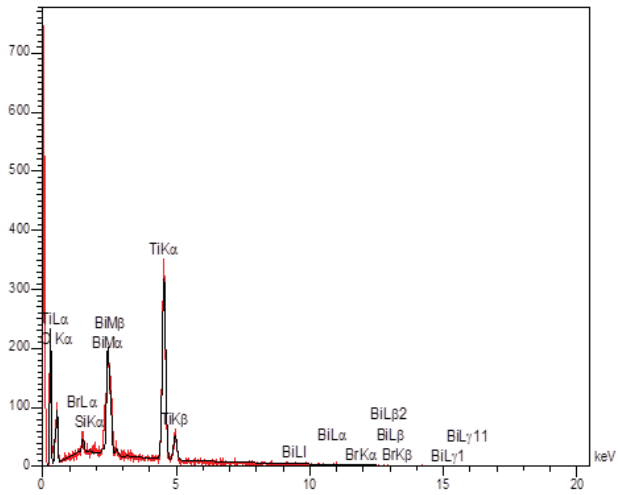

Fig. 4. EDX spectrum of TiO_2/4-CNT/20-BiOBr/10-Bi_2S_3 nanocomposite.

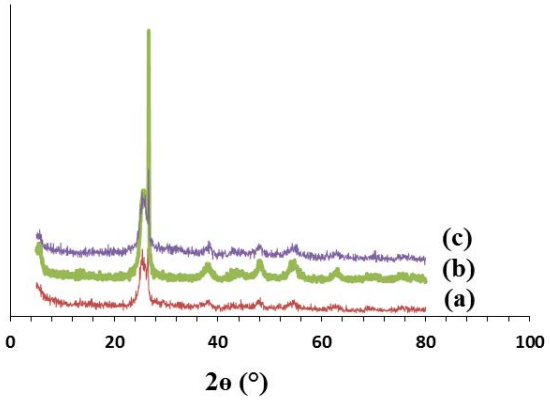

Fig. 5. XRD patterns of (a) TiO_2/4-CNT, (b) TiO_2/4-CNT/20-BiOBr and (c) TiO_2/4-CNT/20-BiOBr/10-Bi_2S_3 nanocomposites.

is higher than the effect of the TiO_2/4-CNT and TiO_2/4-CNT/20-BiOBr/10-Bi_2S_3.

PL spectra have been broadly used to study the recombination of electrons and holes [5]. The recombination rate of electron-hole pairs has affected the PL emission. When the recombination of exited electrons and holes decreases the PL emission intensity is reduced. Fig. 10 shows the PL spectra of TiO_2/4-CNT, TiO_2/4-CNT/20-BiOBr and TiO_2/4-CNT/20-BiOBr/10-Bi_2O_3. All the prepared photocatalysts show a similar pattern at 480 nm. It is obvious that the emission intensity of TiO_2/4-CNT/20-BiOBr and TiO_2/4-CNT/20-BiOBr/10-Bi_2O_3 are weaker than TiO_2/CNT, indicating that the separation efficiency electron and hole pairs are in order of TiO_2/CNT < TiO_2/4-CNT/20-BiOBr < TiO_2/4-CNT/20-BiOBr/10-Bi_2O_3. As a result, TiO_2/4-CNT/20-BiOBr/10-Bi_2O_3 has the

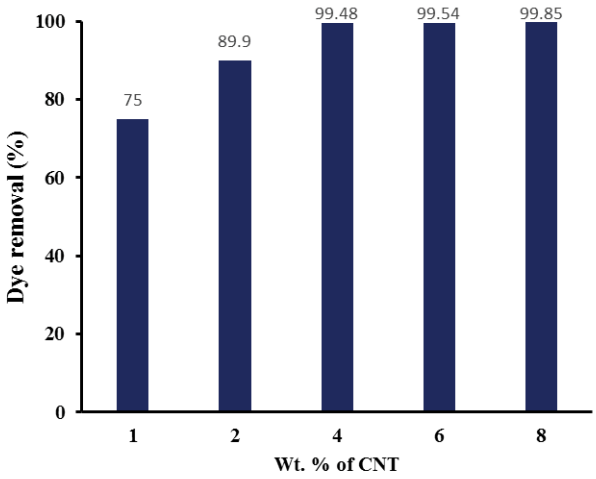

Fig. 7. Effect of CNT loading (%) on AB1721 photodegradation (30 mg/L) at catalyst loading of 1 g/L, the reaction time of 120 min and original pH.

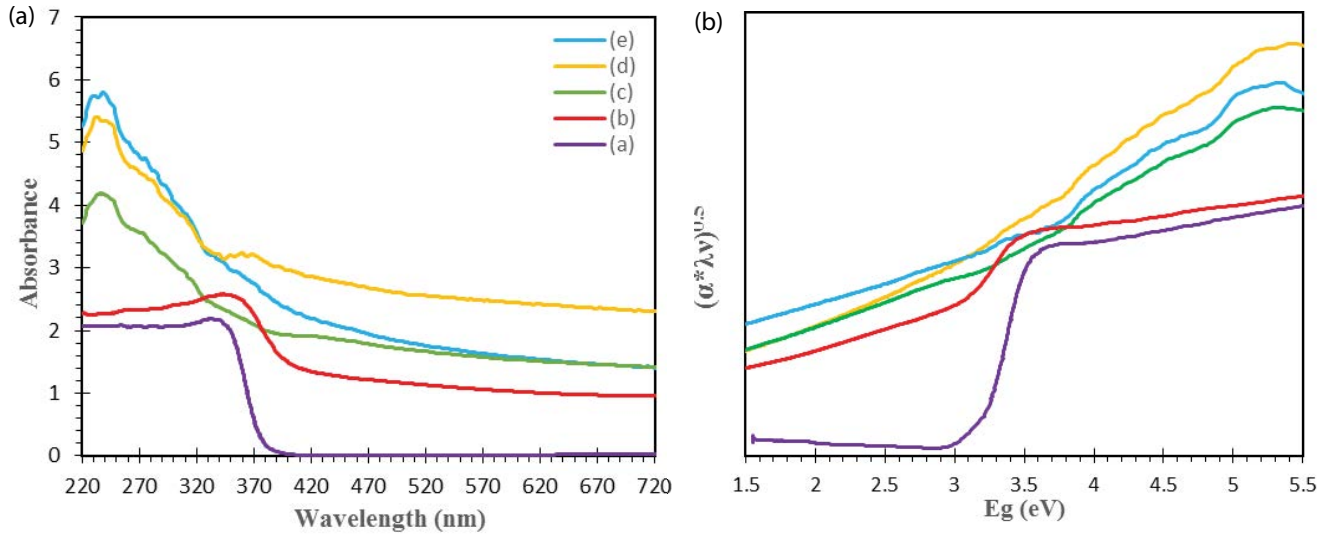

Fig. 6. DRS spectra and Tauc plots of (a) TiO_2, (b) BiOBr, (c) TiO_2/4-CNT, (d) TiO_2/4-CNT/20-BiOBr and (e) TiO_2/4-CNT/20-BiOBr/10-Bi_2S_3 nanocomposites.

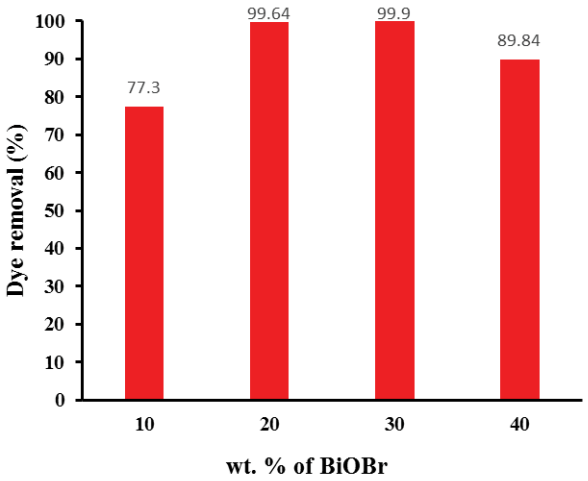

Fig. 8. Effect of BiOBr loading (%) on AB1721 photodegradation (30 mg/L) at catalyst loading of 1 g/L, the reaction time of 60 min and original pH.

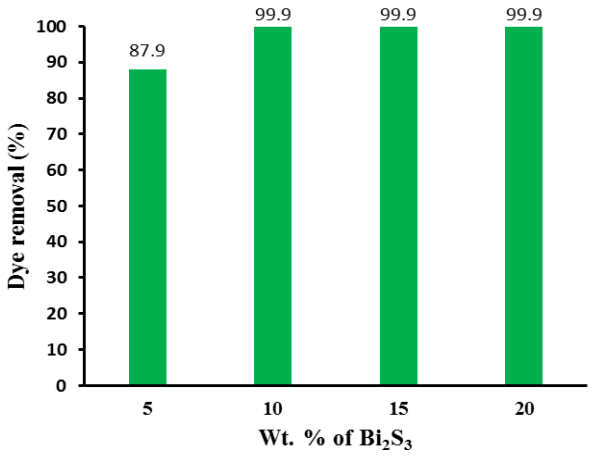

Fig. 9. Effect of Bi_2S_3 loading (%) on AB1721 photodegradation (30 ppm) at catalyst loading 1 g/L, the reaction time of 30 min and original pH.

most photocatalytic activity due to the lower recombination of electrons and hole pairs. From the results of PL and DRS spectra, it can be seen that the TiO_2/4-CNT/20-BiOBr/10-Bi_2O_3 was an optimum photocatalyst due to the most efficient separation and migration of photogenerated electrons and holes and the maximum redshift to the visible range provided by the selected photocatalyst.

3.3. Three-dimensional plots of the regression and optimization process

The results were completely studied using analysis of variance (ANOVA) automatically performed by Design-Expert software (Stat-Ease Inc., version 7.0) (Table 3). ANOVA result indicated that the reduced quadratic model by the probability value of <0.0353 is greatly significant for AB1721 degradation. The fitting of the experimental value to the models was studied by two indicators including *p*-value and *F*-value. If the *p*-value was less than 0.05, the results were statistically significant. There is a good correlation between the predicted and observed data with a correlation coefficient (R^2) of 0.96. The best conditions for the responses yield were determined in terms of actual variables for significant coefficients (*p*-values < 0.05) as described in Eq. (2):

$$\text{Dye removal} = 71.78 - 15.78A + 7.46B - 6.5C + 5.29D - 2.7AB - 2.06AD - 5.10A^2 - 26.70C^2 \quad (2)$$

where *y* represent photodegradation efficiency and *A*, *B*, *C* and *D* refer to the uncoded values of initial dye concentration, catalyst dosage, initial pH and contact time, respectively. The value of adequate precision is 27.08 (>4) which confirms the sufficient signal of the selected model to noise ratio. The coefficient of variance (CV) value indicates the reliability of the model (6.96 less than 10).

Fig. 11 shows the experimental vs. predicted values to determine the correlation between the predicted value

Table 3
ANOVA results for the regression equation describing AB1721 removal efficiency

Source	Sum of squares	df	Mean square	*F*-value	*p*-value
Model	9,700.25	10	970.03	42.48	<0.0001
A-dye concentration	4,672.22	1	4,672.22	204.59	<0.0001
B-catalyst dosage	1,136.06	1	1,136.06	49.75	<0.0001
C-pH	1,917.87	1	1,917.87	83.98	<0.0001
D-Time	416.64	1	416.64	18.24	0.0004
AB	196.00	1	196.00	8.58	0.0086
AC	155.00	1	155.00	6.79	0.017
AD	100.00	1	100.00	4.38	0.044
BC	211.70	1	211.70	9.27	0.05
A^2	120.16	1	120.16	5.26	0.033
D^2	128.44	1	128.44	5.62	0.028
Residual	433.90	21	22.84	–	–
Lack of fit	362.57	16	25.90	1.82	0.2646

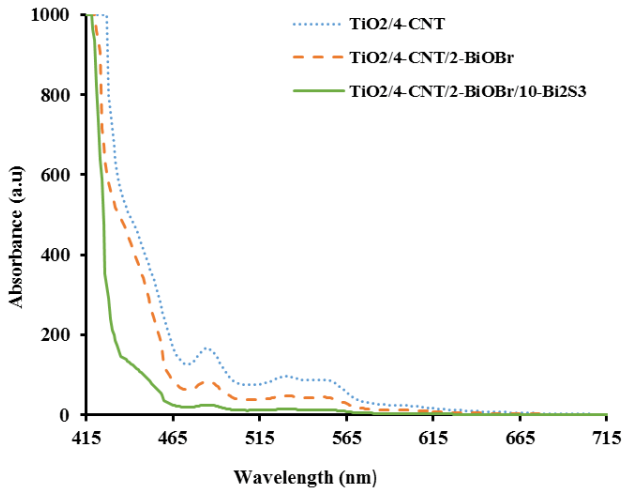

Fig. 10. PL spectra of prepared photocatalysts.

and experimental data. There is a well agreement between the predicted data and experimental AB1721 removal efficiency. Also, the adequacy of the model was confirmed by the normal probability plot of the residuals as represented in Fig 11b. Fig. 11c indicates internally residuals vs. predicted responses which are confirmed the high adequacy of the model or constant variance assumption [27].

3.4. Effect of operational parameters on dye removal

To study the interactive relationships between the independent parameters on the photodegradation, the contour plots are produced. The results of the interactions between the response and the four independent parameters are present in Figs. 12a & b and 13. The variation of the response as a function of dye concentration and irradiation time was illustrated in Fig. 12a which is the contour plot at a pH of 3 and catalyst loading of 1 g/L. As shown in Fig. 12a, with an increase in the initial concentration of AB1721 from 30 to 90 mg/L, the removal efficiency is decreased. This is due to the possibility of interaction between dye molecules with •OH decreases, as a result, a lower dye removal efficiency is accrued, also, an increase in the initial dye concentration leads to more dye adsorption on the catalyst surface and in turn causes the sites inactivation [23]. The combined effect of initial AB1721 concentration and catalyst dosage on the response at a constant pH of 3 and contact time of 40 min was shown in Fig. 12b. It is observed that increasing catalyst loading from 0.5 to 1.0 g/L, improved dye removal efficiency. An increase of TiO_2/4-CNT/20-BiOBr/10-Bi_2S_3 dosage might provide more active sites for the dye molecules to be adsorbed and degraded [22].

The effect of pH and irradiation time on the response at a dye concentration of 30 mg/L and catalyst loading of 1 g/L is plotted in Fig. 13a. The results obtained showed that dye removal was favored at acidic pH conditions. From the literature, pH of zero charge point of TiO_2 NPs in water is 6.2–6.8 [28]. The pH of the zero charge point was achieved by about 4.7 for nanocomposite which is measured by the pH drift method as shown in Fig. 13b [29]. Since the surface

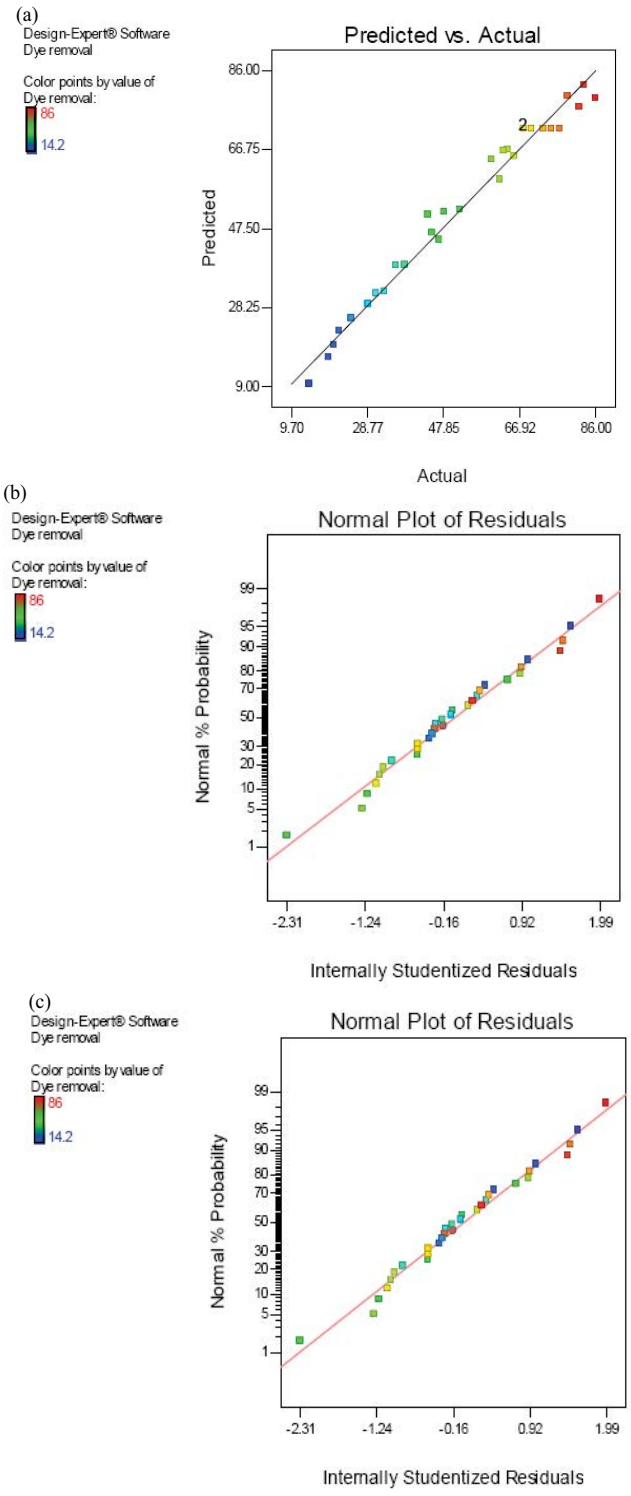

Fig. 11. (a) Predicted vs. actual values, (b) normal probability plots of the residual and (c) internally studentized residual vs. predicted values plots for AB1721 photodegradation efficiency.

of TiO_2/4-CNT/20-BiOBr/10-Bi_2S_3 nanocomposite is positively charged at pH of 3–4.7 while AB1721 molecules have a negative charge sulfite group at this pH. Therefore, the power electrostatic interactions between dye molecules on

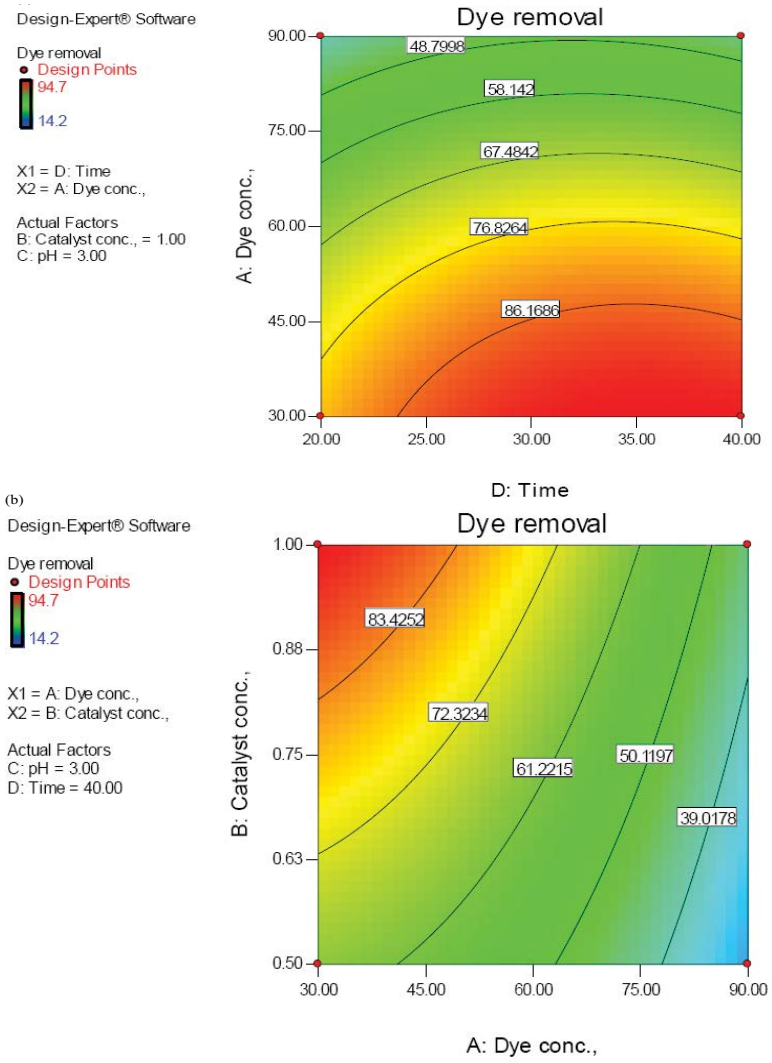

Fig. 12. Contour plot of AB1721 photodegradation efficiency as a function of (a) dye concentration and irradiation time at [catalyst]: 1 g/L and pH of 3 and (b) catalyst loading and dye concentration at pH of 3 and irradiation time of 40 min.

the surface of the photocatalyst was occurred at acidic pH thereby improving photocatalytic activity at acidic pH.

3.5. Reusability results

The TiO_2/4-CNT/20-BiOBr/10-Bi_2S_3 nanocomposite indicates a high efficiency in the photodegradation of AB1721, therefore, its reusability for was also studied by repeating the same experiment at optimum conditions (dye concentration of 30 mg/L, initial pH of 3 and catalyst dosage of 1 g/L) after 40 min. After the first cycle, the suspension of the photocatalyst and treated dye solution was centrifuged and washed with distillation water. A mixture of photocatalyst and distilled water was irradiated in the photoreactor about 1 h and finally dried at 100°C (5 h). As you can see in the Fig. 14, the recycled photocatalyst in the 4 runs with no remarkable loss in its photocatalytic activity. AB1721 removal was 81% after 4 cycles with 77% of the recovered photocatalyst. In order to confirm that this photocatalyst is efficient in reducing the total concentration of all the possible byproducts and AB1721 species, the chemical oxygen demand (COD) test is carried out at the optimal conditions based on the standard methods of water and wastewater experiments. The results showed that COD removal efficiency is achieved at about 99% after 120 min.

4. Conclusions

The new visible driven TiO_2/*a*-CNT/*b*-BiOBr/*c*-Bi_2S_3 photocatalyst with different loadings of CNT (1, 2, 4, 6 and 8 wt.%), BiOBr (10, 20, 30 and 40 wt.%) and Bi_2S_3 (5, 10, 15 and 20 wt.%) were prepared by a hydrothermal method and characterized by BET, FE-SEM/EDX, DRS, XRD, FTIR and PL analyses. The photocatalytic efficiency of the synthesized nanocomposites were investigated with AB1721 photodegradation in a suspended photoreactor. The results show that the photocatalytic activity of TiO_2/4-CNT/20-BiOBr/10-Bi_2S_3 was higher than other samples. DRS results indicated that the TiO_2/4-CNT/20-BiOBr/10-Bi_2S_3 nanocomposite is a visible active photocatalyst with a bandgap of 1.5 eV. PL

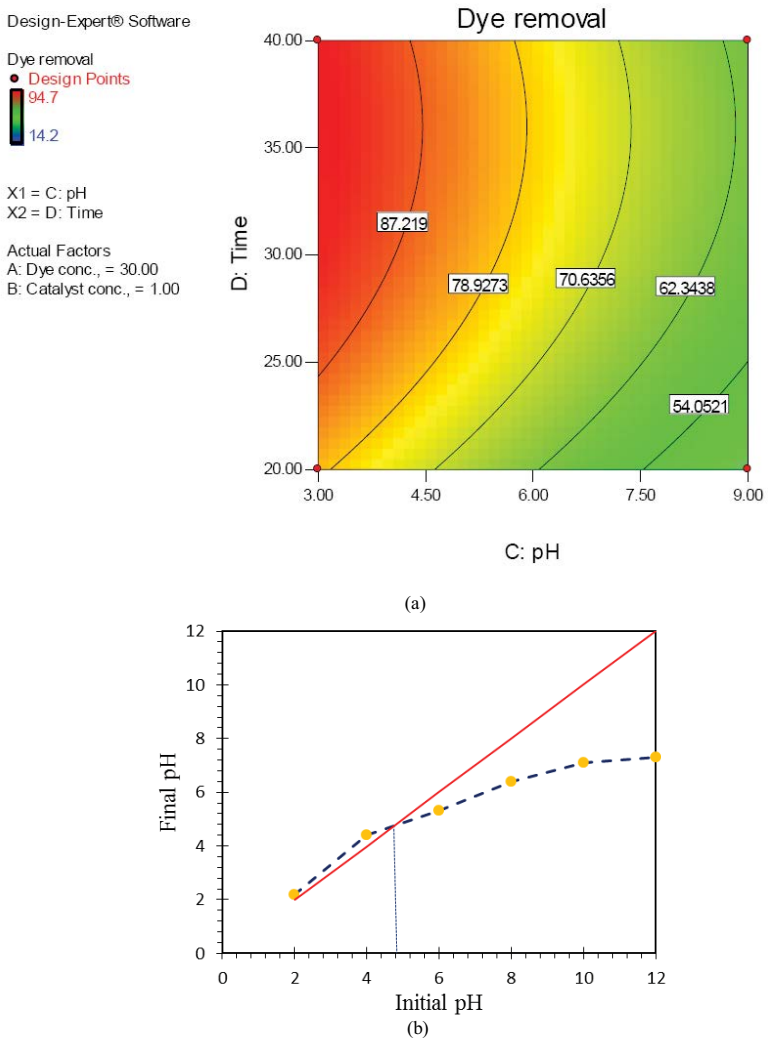

Fig. 13. (a) Contour plot of AB1721 photodegradation efficiency as a function of pH and irradiation time at [dye]: 30 mg/L and [catalyst]: 1 g/L and (b) measurement of the zero charge point for nanocomposite by the pH drift method.

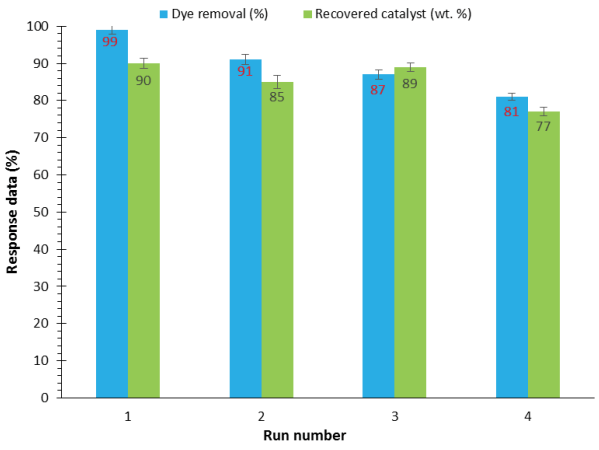

Fig. 14. Reusability results of TiO_2/4-CNT/20-BiOBr/10-Bi_2O_3 nanocomposite at pH of 3, catalyst loading of 1 g/L and dye concentration of 30 mg/L.

results shown that the TiO_2/4-CNT/20-BiOBr/10-Bi_2S_3 had a lower recombination rate of electrons/holes, as a result, it has more photocatalyst activity than other photocatalysts. The increasing dye concentration and pH values reduce the photocatalytic removal efficiency. The positive effect of catalyst loading and irradiation time on photocatalytic removal was also observed during the photodegradation process. Complete decolorization was achieved at a dye concentration of 30 mg/L, initial pH of 3 and catalyst dosage of 1 g/L after 40 min while COD removal was 99% after 120 min.

References

[1] H. Zangeneh, A.A. Zinatizadeh, M. Habibi, M. Akia, M.H. Isa, Photocatalytic oxidation of organic dyes and pollutants in wastewater using different modified titanium dioxides: a comparative review, J. Ind. Eng. Chem., 26 (2015) 1–36.

[2] L.G. da Silva, R. Ruggiero, P.D.M. Gontijo, R.B. Pinto, B. Royer, E.C. Lima, T. Calvete, Adsorption of brilliant red 2BE dye from water solutions by a chemically modified sugarcane bagasse lignin, Chem. Eng. J., 168 (2011) 620–628.

[3] H. Zangeneh, M. Farhadian, A.A. Zinatizadeh, N (Urea) and C-N (L-Asparagine) doped TiO_2-CuO nanocomposites: fabrication, characterization and photodegradation of direct red 16, J. Environ. Chem. Eng., 8 (2020) 103639.
[4] M. Aram, M. Farhadian, A.R. Solaimany Nazar, S. Tangestaninejad, P. Eskandari, B.H. Jeon, Metronidazole and cephalexin degradation by using of Urea/TiO_2/$ZnFe_2O_4$/clinoptiloite catalyst under visible-light irradiation and ozone injection, J. Mol. Liq., 304 (2020) 112764.
[5] E. Rafiee, E. Noori, A.A. Zinatizadeh, H. Zanganeh, A new visible driven nanocomposite including Ti-substituted polyoxometalate/TiO_2: synthesis, characterization, photodegradation of azo dye process optimization by RSM and specific removal rate calculations, J. Mater. Sci.-Mater. Electron., 29 (2018) 20668–20679.
[6] C.-Y. Yen, Y.-F. Lin, C.-H. Hung, Y.-H. Tseng, C.-C.M. Ma, M.-C. Chang, H. ShaO, The effects of synthesis procedures on the morphology and photocatalytic activity of multi-walled carbon nanotubes/TiO_2 nanocomposites, Nanotechnology, 19 (2008) 045604.
[7] C.-H. Wu, C.-Y. Ku, S.-T. Chen, Synergistic effects between TiO_2 and carbon nanotubes (CNTs) in a TiO_2/CNTs system under visible light irradiation, Environ. Technol., 34 (2013) 2513–2519.
[8] P. Serp, M. Corrias, P. Kalck, Carbon nanotubes and nanofibers in catalysis, Appl. Catal., A, 253 (2003) 337–358.
[9] Y. Yao, G. Li, S. Ciston, R.M. Lueptow, K.A. Gray, Photoreactive TiO_2/carbon nanotube composites: synthesis and reactivity, Environ. Sci. Technol., 42 (2008) 4952–4957.
[10] D. Zhao, C.-F. Yang, Recent advances in the TiO_2/CdS nanocomposite used for photocatalytic hydrogen production and quantum-dot-sensitized solar cells, Renewable Sustainable Energy Rev., 54 (2016) 1048–1059.
[11] S. Kumar, S. Sharma, S. Sood, A. Umar, S.K. Kansal, Bismuth sulfide (Bi_2S_3) nanotubes decorated TiO_2 nanoparticles heterojunction assembly for enhanced solar light driven photocatalytic activity, Ceram. Int., 42 (2016) 17551–17557.
[12] X. Tan, X.L. Li, T. Yu, Y. Zhao, Preparation and photocatalytic activity of BiOBr/TiO_2 heterojunction nanocomposites, Trans. Tianjin Univ., 22 (2016) 211–217.
[13] X.F. Chang, M.A. Gondal, A.A. Al-Saadi, M.A. Ali, H.F. Shen, Q. Zhou, J. Zhang, M.P. Du, Y.S. Liu, G.B. Ji, Photodegradation of Rhodamine B over unexcited semiconductor compounds of BiOCl and BiOBr, J. Colloid Interface Sci., 377 (2012) 291–298.
[14] G.H. Jiang, X.H. Wang, Z.Z. Wei, X. Li, X.G. Xi, R.B. Hu, B.L. Tang, R.J. Wang, S. Wang, T. Wang, W.X. Chen, Photocatalytic properties of hierarchical structures based on Fe-doped BiOBr hollow microspheres, J. Mater. Chem. A, 1 (2013) 2406–2410.
[15] M. Shang, W.Z. Wang, L. Zhang, Preparation of BiOBr lamellar structure with high photocatalytic activity by CTAB as Br source and template, J. Hazard. Mater., 167 (2009) 803–809.
[16] W.W. Lin, X. Wang, Y.H. Wang, J.Y. Zhang, Z. Lin, B.T. Zhang, F. Huang, Synthesis and facet-dependent photocatalytic activity of BiOBr single-crystalline nanosheets, Chem. Commun., 53 (2017) 4861.
[17] D. Zhang, J. Li, Q.G. Wang, Q.S. Wu, High {001} facets dominated BiOBr lamellas: facile hydrolysis preparation and selective visible-light photocatalytic activity, J. Mater. Chem. A, 1 (2013) 8622–8629.
[18] Y.C. Feng, L. Li, J.W. Li, J.F. Wang, L. Liu, Synthesis of mesoporous BiOBr 3D microspheres and their photodecomposition for toluene, J. Hazard. Mater., 192 (2011) 538–544.
[19] J.L. Qiao, Q.Y. Wang, J.X. Ye, Y.K. Xiao, Enhancing photoelectrochemical performance of TiO_2 nanotube arrays by CdS and Bi_2S_3 co-sensitization, J. Photochem. Photobiol., A, 319 (2016) 34–39.
[20] A. Witek-Krowiak, K. Chojnacka, D. Podstawczyk, A. Dawiec, K. Pokomeda, Application of response surface methodology and artificial neural network methods in modelling and optimization of biosorption process, Bioresour. Technol., 160 (2014) 150–160.
[21] M.J.K. Bashir, H.A. Aziz, M.S. Yusoff, M.N. Adlan, Application of response surface methodology (RSM) for optimization of ammoniacal nitrogen removal from semi-aerobic landfill leachate using ion exchange resin, Desalination, 254 (2010) 154–161.
[22] H.Y. Xu, L.C. Wu, H. Zhao, L.G. Jin, S.Y. Qi, Synergic effect between adsorption and photocatalysis of metal-free g-C_3N_4 derived from different precursors, PLoS one, 10 (2015) e0142616.
[23] E. Rafiee, E. Noori, A.A. Zinatizadeh, H. Zanganeh, Photocatalytic degradation of phenol using a new developed TiO_2/graphene/heteropoly acid nanocomposite: synthesis, characterization and process optimization, RSC Adv., 6 (2016) 96554–96562.
[24] S. Xiao, W. Zhu, P.J. Liu, F.F. Liu, W.R. Dai, D.Q. Zhang, W. Chen, H.X. Li, CNTs threaded (001) exposed TiO_2 with high activity in photocatalytic NO oxidation, Nanoscale, 8 (2016) 2899–2907.
[25] S. Boumaza, B. Bellal, A. Boudjemaa, M. Trari, Photodegradation of orange G by the hetero-junction x% Bi_2S_3/TiO_2 under solar light, J. Sol. Energy, 139 (2016) 444–451.
[26] X.-X. Wei, C. Haitao, G. Shaoqing, Z. Liangfu, W. Li, Hybrid BiOBr–TiO_2 nanocomposites with high visible light photocatalytic activity for water treatment, J. Hazard. Mater., 263 (2013) 650–658.
[27] P. Eskandari, M. Farhadian, A.R. Solaimany Nazar, B.-H. Jeon, Adsorption and photodegradation efficiency of TiO_2/Fe_2O_3/PAC and TiO_2/Fe_2O_3/zeolite nanophotocatalysts for the removal of cyanide, Ind. Eng. Chem. Res., 58 (2019) 2099–2112.
[28] E.N. El. Qada, S.J. Allen, G.M. Walker, Adsorption of methylene blue onto activated carbon produced from steam activated bituminous coal: a study of equilibrium adsorption isotherm, Chem. Eng. J., 124 (2006) 103–110.
[29] J. Saien, M. Asgari, A.R. Soleymani, N. Taghavini, Photocatalytic decomposition of direct red 16 and kinetics analysis in a conic body packed bed reactor with nanostructure titania coated Raschig rings, Chem. Eng. J., 151 (2009) 295–301.